European Conference on Computational Fluid Dynamics
ECCOMAS CFD 2006
P. Wesseling, E. Oñate and J. Périaux (Eds)

OPTIMIZATION OF BLENDED WING BODY AIRCRAFT BY AN AUTOMATIC CFD DRIVEN DESIGN TOOL

Sergey Peigin* **and Boris Epstein†**

*Israel Aircraft Industries, Israel
e-mail: speigin@iai.co.il
†The Academic College of Tel-Aviv Yaffo, Israel
e-mail: epstein@mta.ac.il

Key words: Blended Wing Body, Aerodynamic Shape Optimization, Constarint Handling, Genetic Algorithm

Abstract. *Blended wing body (BWB) aircraft has aroused considerable interest as a potential candidate for future large subsonic transport air-vehicles. In this paper, we present the results of one- and multi-point multi-constrained optimization of a BWB configuration for minimum total drag. The optimization technique includes a new strategy for efficient handling of nonlinear constraints in the framework of Genetic Algorithms, scanning of the optimization search space by a combination of full Navier-Stokes computations with Reduced Order Methods and multilevel parallelization of the whole computational framework. The assessment of the results shows that the proposed technology allows the design of feasible aerodynamic shapes which possess a low drag at cruise conditions, satisfy a large number of geometrical and aerodynamic constraints and offer good off-design performance in markedly different flight conditions.*

1 INTRODUCTION

The blended wing body (BWB) aircraft is a tailless design which integrates the wing and the fuselage. The conceptual advantage of this configuration lies in its lower wetted area to volume ratio and lower interference drag as compared to the conventional transport aircraft. A BWB has an additional advantage: lift and payload are much more in line. This reduces blending moments and therefore structural weight. The concept goes back to non-conventional flying wing designs originally proposed almost 60 years ago [1]. The BWB configuration concept is a radical change from the dominant design where a wing is combined with a cylinder-type fuselage, and the longitudinal stability of the aircraft is maintained by means of a tail.

In the late 1990s, the BWB aircraft was considered in the US as a potential candidate for future large subsonic transport aircraft [2]-[3]. The project involved a number of industrial and academic establishments, including National Aeronautics and Space Administration (NASA). The comprehensive survey of these activities may be found in [4].

A serious effort was also mounted in Europe to design their version of a BWB configuration. Starting in 2002, a European Commission funded a project aimed at the design and optimization of BWB aircraft [5]. A progressive study of the aerodynamic performance for the corresponding BWB configuration may be found in Ref. [6], where a BWB geometry without fins was considered.

It is the authors' opinion, that computational fluid dynamics (CFD) and CFD-driven optimization methods could play a great role in fulfilling the aerodynamic objectives of the above projects. However, prior to the last few years, CFD driven optimization had a limited impact on the aircraft design practice especially in the case of complex 3D aerodynamic shapes similar to BWB.

The reason why the optimization tools are still not being exploited as one would like in the design process is partially due to the following three reasons. First, only recently computational simulation has been allowed for relatively accurate drag prediction (within the accuracy of 2-3 aerodynamic counts) required in engineering practice (see the results of the 2nd AIAA Drag Prediction Workshop [7]). Second, the industrial optimization of aerodynamic shapes necessitates high-dimensional search spaces, and a large number of non-linear constraints are placed upon a desired optimum.

Last but not least, the huge computational volume needed for optimization (and the corresponding huge computational resources) presents a major obstacle to the incorporation of CFD based optimization into the core of the industrial aerodynamic design.

The aerodynamic optimization of BWB configurations presents additional difficulties compared to the optimization of conventional aircraft configurations due to an essential increase in the number of design variables and to the necessity to comply with a number of additional aerodynamic constraints coming from the stability considerations.

In Ref. [8] an efficient and robust algorithm for CFD driven optimization of three-dimensional aerodynamic wings, based on Genetic Algorithms search and full Navier-Stokes computations, was proposed by the authors'. In this context, the main objective of this paper is to apply the method [8] to the one- and multi-point multi-constrained optimization of a BWB configuration for minimum total drag, and to analyze the influence of the aerodynamic parameters of the problem on the optimal configuration. It was demonstrated that the optimization method allows the design of feasible aerodynamic shapes which possess a low drag at cruise conditions, satisfy a large number of geometrical and aerodynamic constraints and offer good off-design performance in markedly different flight conditions such as take-off conditions and high Mach zone.

2 STATEMENT OF THE PROBLEM

In the design practice, the parameters of optimization originate from the conceptual design stage which provides the initial geometry definition and the aerodynamic performance data. The aerodynamic specification includes the prescribed cruise lift, Mach number, altitude and maximum allowed drag values which will meet the goals of the aircraft mission (such as range, payload, fuel volume etc).

The desired optimal geometry is sought from a class of solutions which satisfy different geometrical, aerodynamic and multidisciplinary constraints (which also originate from the stage of conceptual design). Specifically, airfoil thickness, pitching moment, C_L^{max} at the take-off conditions are normally constraint.

The design objective is to develop an aircraft configuration with as low a drag at cruise conditions as possible which, at the same time, satisfies the above constraints. This is accomplished through a CFD-based solution of the properly formulated multi-point constrained optimization problem.

In the problem formulation, the first crucial issue is the choice of the objective function. We assume that the drag coefficient C_D of a configuration (at constant reference area) is a sensitive and reliable indicator of its aerodynamic performance and thus we employ C_D as the objective function of the considered optimization problem.

The next important issue is the implementation of constraints in the optimization algorithm. Where possible, the constraints should be satisfied accurately (up to machine accuracy) and directly, while the remaining constraints should be converted into alternative constraints which can be expressed in terms of drag.

For example, we should satisfy the geometrical constraints and such aerodynamic constraints as the prescribed lift coefficient exactly while the requirement of a sufficiently high C_L^{max} at the take-off conditions should be reformulated in terms of drag at the corresponding flight conditions. This means that instead of maximizing C_L^{max}, we minimize C_D at a fixed C_L value close to that needed to meet the specified aerodynamic requirements.

Finally in order to ensure the accuracy of optimization we require that for any geometry feasible from the constraints' viewpoint, the value of the objective (cost) function remains exactly equal to the value of the drag coefficient without any penalization.

Based on the above principles, the mathematical formulation of the optimization problem may be expressed as follows.

The objective of the general multipoint optimization problem is to minimize the weighted combination C_D^{wtd} of drag coefficients at the main design and secondary design points (flight conditions)

$$C_D^{wtd} = \sum_{k=1}^{K} w_k C_D(k)$$

where K is the total number of the design points. The specific values of the weight factors w_k reflect the relative importance of the design points coming from the aerodynamic practice. The main design point deals with cruise conditions. Secondary design points are chosen in order to ensure good off-design aerodynamic performance. Specifically, the following secondary design points may be used: 1) a higher Mach design point (to improve Mach drag rise behaviour); 2) a higher C_L design point at the cruise Mach number (to improve climb behaviour) and 3) a design point corresponding to the take-off conditions.

The solution is sought in the class of wing shapes subject to the following classes of constraints:

1) Aerodynamic constraints such as prescribed constant total lift coefficient $C_L^*(k)$ and minimum allowed pitching moment $C_M^*(k)$:

$$C_L(k) = C_L^*(k), \quad C_M(k) \geq C_M^*(k) \tag{1}$$

Thus we assume that $C_L^*(k)$ and $C_M^*(k)$ are not a function of design variables.

2) Geometrical constraints on the shape of the wing surface in terms of properties of sectional airfoils at the prescribed wing span locations: relative thickness $(t/c)_i$, relative local thickness $(\Delta y/c)_{ij}$ at the given chord locations $(x/c)_{ij}$ (beam constraints), relative radius of leading edge $(R/c)_i$, trailing edge angle θ_i:

$$(t/c)_i \geq (t/c)_i^*, \quad (\Delta y/c)_{ij} \geq (\Delta y/c)_{ij}^*, \quad (R/c)_i \geq (R/c)_i^*, \quad \theta_i \geq \theta_i^* \tag{2}$$
$$i = 1, ..., N_{ws}, \quad j = 1, ..., N_{bc}(i)$$

where N_{ws} is the total number of sectional airfoils' subject to optimization, $N_{bc}(i)$ is the total number of beam constraints at section i, and values $(t/c)_i^*$, $(\Delta y/c)_{ij}^*$, θ_i^*, $(R/c)_i^*$, C_L^* and C_M^* are prescribed parameters of the problem. Though only the above listed constraints were taken into account in the present work, it is possible (in the framework of the proposed method) to impose additional geometrical constraints, such as minimum allowed wing volume.

Thus in the present work the total number of considered constraints N_{cs} is equal to

$$N_{cs} = 2 \times K + 3 \times N_{ws} + \sum_{i=1}^{N_{ws}} N_{bc}(i)$$

3 OPTIMIZATION METHOD

As a CFD driver of the optimization process the numerical solution of the full Navier-Stokes equations is used.

The use of a consistently accurate Navier-Stokes solver is a necessary requirement imposed upon any accurate optimization of aerodynamic shapes. Note that the optimization method requires not only the exact evaluations of the objective function (in our case, the total drag), but also accurate evaluations of additional sensitive aerodynamic characteristics needed in order to satisfy the aerodynamic constraints.

To do this, the numerical noise must be significantly lower than, for example, the difference in the values of drag for geometrically close but distinctly different aerodynamic shapes tested in the process of optimization.

The failure to fulfill the above requirement leads to the incorrect estimation of shapes in terms of the objective function (regardless of the optimization technique) and thus may result in the failure of the whole optimization process.

In the present work, numerical solutions of the full Navier-Stokes equations are obtained by means of the multiblock code NES [9]. The numerical method employs structured point-to-point matched grids and is based on the Essentially Non-Oscillatory (ENO)

concept with a flux interpolation technique [10] which allows accurate estimation of sensitive aerodynamic characteristics such as lift, pressure drag, friction drag and pitching moment. The code ensures high accuracy of the Navier-Stokes computations, possesses high robustness for a wide range of flows and geometrical configurations and thus keeps the numerical noise to the low level [11].

The present optimization technique [8] is based on the use of Genetic Algorithms (GAs). As a basic algorithm, a variant of the floating-point GA [12] is used.

In the considered optimization problem, the presence of constraints has a great impact on the solution. This is due to the fact that the optimal solution does not represent a local minimum in the conventional sense of the word. Instead, it is located on an intersection of hypersurfaces of different dimensions, generated by linear and non-linear constraints [13]. Additionally, the problem of finding such an extremum is essentially complicated by the fact that these hypersurfaces, which bound the feasible search space, are not known in advance.

To make the optimum search efficient, we changed the conventional search strategy by employing search paths through both feasible and infeasible points. To implement the new strategy, it was proposed to extend the search space by evaluating (in terms of fitness) the points, which do not satisfy the constraints imposed by the optimization problem. A needed extension of an objective function may be implemented by means of GAs due to their basic property: contrary to classical gradient-based optimization methods, GAs are not confined to only smooth extensions (for more detail see [13]).

One of the main weaknesses of GAs lies in their poor computational efficiency. This prevents their practical use in the case where the evaluation of the cost function is computationally expensive as it happens in the framework of the full Navier-Stokes model. To overcome this, we introduce an intermediate "computational agent" - a computational tool which, on the one hand is based on a very limited number of exact evaluations of objective function and, on the other hand provides a fast and reasonably accurate computational feedback in the framework of GAs search.

We construct a computational agent by means of a Reduced-Order Models (ROM) approach in the form of Local Approximation Method (LAM). With the ROM-LAM method, the solution functionals which determine a cost function and aerodynamic constraints (such as pitching moment, lift and drag coefficients), are approximated by a local data base. The data base is obtained by solving the full Navier-Stokes equations in a discrete neighbourhood of a basic point (basic geometry) positioned in the search space. Note, that for the basic geometry, the design C_L is achieved by varying the angle of attack of the configuration.

So on the one hand, the number of exact estimations of the objective function (full Navier-Stokes solutions) is proportional to the dimension of the search space. On the other hand, the computational volume required to provide approximate estimates of the objective function in the framework of GAs optimum search, is negligible.

To overcome the approximate nature of the search, the search is simultaneously per-

Case No.	C_L^*	M	w_i	C_M^*
$CaseBWB\_1$	0.41	0.85	1.0	-0.300
$CaseBWB\_2$	0.41	0.85	1.0	-0.075
$CaseBWB\_3$	0.41	0.85	0.70	-0.075
	0.41	0.87	0.25	-0.100
	1.63	0.20	0.05	-0.330
$CaseBWB\_4$	0.41	0.85	0.95	-0.075
	1.63	0.20	0.05	-0.330

Table 1: Blended wing body aircraft. Optimization conditions and constraints.

formed on a number of embedded search domains, and the set of thus obtained optimal shapes are verified through full Navier-Stokes evaluations.

Besides, in order to ensure the global character of the search, it is necessary to overcome the local nature of the above approximation. For this purpose it is suggested to perform iterations in such a way that in each iteration, the result of optimization serves as the initial point for the next iteration step (further referred to as optimization step). The specific algorithm is described in Ref. [8].

Additionally, multilevel parallelization of the whole optimization framework allows one to make use of the computational power supplied by massively parallel processors and thus to essentially improve the computational efficiency (for more detail see [14]).

4 DISCUSSION OF RESULTS

In this section we present the results of one- and multi-point drag minimization of a blended wing body aircraft configuration without the influence of trailing-edge devices. The initial (tailless) geometry of the aircraft was proposed within the European Commission funded project Ref. [5] and may be found in Ref. [6].

The main design point was $C_L = 0.41$, $M = 0.85$ (as in [6]). The secondary design points were chosen at $M = 0.87$ (high Mach cruise conditions) and at $M = 0.2$ (take-off conditions). The design Reynolds number Re was equal to $5.41 \cdot 10^6$ (assuming that the characteristic length in the Reynolds number definition is equal to $1m$). The geometrical constraints were imposed on thickness ($(t/c)_i^* = (t/c)_i^b$), leading edge radius ($(R/c)_i^* = (R/c)_i^b$) and trailing edge angle ($\theta_i^* = \theta_i^b$) as well as two local thickness constraints per section. An additional (aerodynamic) constraint was placed upon the pitching moment.

The design conditions and constraints are summarized in Table 1, while the results of optimization are given in Table 2. The corresponding optimal shapes are designated by $CaseBWB\_1$ to $CaseBWB\_4$.

For the transonic BWB aircraft configuration, NES provides accurate asymptotically converged estimates of aerodynamic coefficients with the fine level grids containing $209 \times 57 \times 41$ computational points in the streamwise, spanwise and normal to surface direction,

respectively.

Unfortunately, such computations, though feasible for a single optimization, are too heavy to be used in the industrial framework. To overcome this limitation, we used the invariance of the hierarchy of objective function values on the medium and fine grids Ref. [8]. It is feasible if the grid coarsening preserves the hierarchy of fitness function values on the search space (that is, the relation of order is invariant with respect to grid coarsening). This means that the objective function Q_c defined on a coarse grid can be used for solution of the optimization problem, if for every pair of points x_1, x_2 belonging to the search space, the relation of order between the values of an objective function Q_c on a coarse grid implies the same order relation for the objective function Q_f defined on a fine grid. For 2D optimization, the feasibility of the above approach was confirmed in Ref. [13].

It appeared that the two times coarser in each direction ($105 \times 29 \times 21$) grids satisfy the invariance conditions. This allowed us to use meshes with such a resolution for optimization purposes.

One single-point optimization requires an overnight run on the above cluster while a typical three-point optimization which includes one main design point and two secondary design points, may take as much as 1.5-2 days.

Note, that though the CFD computations employed in the optimization stream were based on the medium grid resolution, all the aerodynamic data listed below were obtained on the fine grid.

4.1 One-point optimization

Before discussing the obtained results we compare the present results with other published results. The considered BWB aircraft configuration was the subject of a previous optimization within a European project [5]. The results of this single-point optimization at the main cruise conditions ($C_L = 0.41$, $M = 0.85$) were reported in [6]. In [6] the optimization with a gradient method, was based on the solution of the Euler equations and the corresponding adjoint equations, while the final optimal shape was verified through the solution of the full Navier-Stokes equations.

The comparison of the results in Ref. [6] with those obtained by the present method (one-point optimization $CaseBWB\_1$) is as follows. In Ref. [6], the reduction of 26 aerodynamic counts was achieved (out of the initial 285.5 counts). The corresponding optimization by the present method yielded the reduction of 52.5 counts (out of the initial 247 counts).

In order to obtain a better assessment of the optimization results, it is worthwhile to analyze the aerodynamic behaviour of the baseline BWB configuration (taken from [6]). A CFD analysis (performed by the code NES [9]) at transonic flight conditions provides evidence to strong shocks on most of the aircraft upper surface (see Fig. 1).

The computation at $C_L = 0.41$, $M = 0.85$ yields 247 counts. At this flight point, the theoretical induced drag (taking into account the difference between the wetted and the

Case	C_D (counts) at $M = 0.85$, $C_L = 0.41$	C_D (counts) at $M = 0.87$, $C_L = 0.41$	C_L^{max} at $M = 0.20$
Baseline	247.0	287.0	1.63
$CaseBWB\_1$	194.5	207.4	1.51
$CaseBWB\_2$	196.4	213.4	1.47
$CaseBWB\_3$	196.7	202.5	1.76
$CaseBWB\_4$	196.6	216.6	1.67

Table 2: Blended wing body aircraft. Optimization results.

reference wing areas) is estimated to be about 75 counts. On the other hand, the zero lift total drag for the same configuration, for a purely subsonic flow at $M = 0.60$, is equal to 115 counts. Thus the baseline configuration possesses a fair amount of wave drag which gives a good promise that a proper shape optimization should result in a significant drag reduction. This conclusion may be also confirmed by the computation at $C_L = 0.41$, $M = 0.60$ where the total drag is equal to 190.6 counts, which complies with the previous wave drag estimate at the main design point (above 50 counts).

The first optimization case labeled as $CaseBWB\_1$, is a single-point optimization with unconstrained pitching moment. The total drag of the optimal configuration amounts to 194.5 counts (compared to the initial 247.0 counts) with the pitching moment $C_M = -0.300$ compared to the baseline $C_M = -0.075$. The comparison of sectional pressure distributions for the baseline shape (Fig. 1) with the optimized ones for $M = 0.85$ (Fig. 2) shows that the original strong shock was virtually eliminated by the optimization. This resulted in a total drag level close to the above estimated low bound (about 191 aerodynamic counts). Note, that the shock elimination phenomenon is not pointwise: this trend is also clearly observed at a higher Mach value $M = 0.87$.

The analysis of the iterative optimization stream (see Fig. 3) demonstrates that the main means of drag minimization is related to the build up of a highly cusped trailing edge shape. Note, that this trend is widely used in practical aerodynamic design.

At the same time, though the optimization ($CaseBWB\_1$) was highly successful in terms of drag reduction, the corresponding C_M value appeared unacceptable due to stability considerations. This necessitated another one-point optimization (labeled $CaseBWB\_2$) at the conditions of $CaseBWB\_1$ with an additional constraint imposed on the pitching moment in order to keep it to the original level. The results of the optimization were as follows. The total drag was reduced to 196.4 counts, while the pitching moment of the optimal aircraft configuration was exactly equal to the original one ($C_M = -0.075$).

The analysis of the achieved results allows one to draw the following conclusions. First, the drag penalty due to the limitation of pitching moment amounted to only 1.9 counts. Second, though both optimal configurations yield very close total drag values, the corresponding shapes are markedly different (see Fig. 4). This may be explained in the

following way. In order to comply with the constraint on the pitching moment, an essentially higher loading of the leading edge region of the aircraft (compared to the unconstrained optimization $CaseBWB\_1$) should be achieved. This means that in this case, the drag minimization can not be accomplished by the same aerodynamic design techniques which were successfully used by the optimizer in $CaseBWB\_1$. Indeed, as it can be seen from Fig. 4, the present optimization method discovered new aerodynamic resources and formed a drooped leading edge shape, which is another well known design feature.

4.2 Multi-point optimization

From the pointwise optimization view, the results achieved in $CaseBWB\_2$, are quite successful, because at the design conditions, the drag was reduced by 50.6 counts (coming close to the theoretical minimum) while keeping all the constraints (including that of the pitching moment) to the required level. However, the final decision on the feasibility of an optimal shape, should be made only upon the configuration testing at off-design conditions. Specifically, at least three following off-design characteristics should be checked. First, the drag behaviour at higher-than-cruise lift conditions (at the cruise Mach value). Second, the quality of Mach drag divergence at the considered cruise $C_L = 0.41$. And finally, the value of C_L^{max} at the take-off conditions should be tested.

With this end in view, the optimal BWB aircraft configuration ($CaseBWB\_2$) was analyzed. The results show that the drag behaviour at higher C_L (the first test) is quite satisfactory: at $C_L = 0.444$, only 2-3 wave drag counts are added. As for the above second and third off-design conditions, the following analysis demonstrates that there is room for improvement. Specifically, at $M = 0.87$, $C_L = 0.41$ about 17 counts of wave drag were added compared to $M = 0.85$, while C_L^{max} at $M = 0.2$ was equal to 1.47 (compared to $C_L^{max} = 1.63$ for the initial baseline BWB configuration).

In this connection the following multi-point optimizations were carried out: $CaseBWB\_3$, which includes the main design point and two secondary design points at high Mach and at take-off conditions, and $CaseBWB\_4$, which combines the main design point and the take-off design point (see Table 1).

Let us consider the results of the three-point optimization. At the main flight conditions, the optimal shape yielded 196.7 counts which is rather close to the theoretical minimum (see the above discussion). The surface pressure distribution on the upper surface of the optimal configuration is compared with this of the baseline geometry in Figs. 5-6. It can be assessed that the optimization considerably changed the configuration loading by removing the strong shocks present in the flow over the original aircraft shape.

The off-design performance at higher than cruise lift coefficients (at $M = 0.85$) is satisfactory: for example, the drag value at $C_L = 0.45$ is equal to 214.0 counts which means that the additional wave drag (compared to the cruise $C_L = 0.41$) is only about 2-3 aerodynamic counts.

As for the two-point optimization ($CaseBWB\_4$), the results were as follows: C_L^{max} increased to 1.671 (thus removing the drawback of $CaseBWB\_2$ at the take-off conditions)

while the total drag at the main design point was equal to 196.6 counts (in fact, preserving the gain in drag value achieved in $CaseBWB\_2$).

At the same time, the drag value at $M = 0.87$ was even higher than in the one-point optimization of $CaseBWB\_2$ (216.6 counts compared to 213.4 counts), thus indicating the need for a three-point optimization.

The next important issue is the aerodynamic performance of the optimal shape at high Mach values. As it was already mentioned above, the one- and two-point optimizations resulted in approximately the same value of C_D at $M = 0.87$ - about 215.0 counts. The three-point optimization (in which higher than cruise Mach flight conditions are additionally taken into account), allows to improve the Mach drag rise characteristics of the BWB aircraft. Specifically, the total drag value at $C_L = 0.41$, $M = 0.87$ became 202.5 counts (a reduction of 12.5 counts compared with the previous optimizations). The analysis of the corresponding pressure distributions (see Figs. 7-8) shows that the main mechanism which allowed to reach a significant drag reduction, consists in the successful shock wave destruction.

Alongside surface aerodynamic characteristics, an important source of aerodynamic data needed for the analysis of flow structures, are off-body iso-Mach contours. The corresponding sectional Mach distributions over the baseline configuration and the optimal one ($CaseBWB\_3$) for the free-stream $M = 0.85$ are given in Figs. 9 - 10.

Already at the symmetry plane, the baseline configuration is characterized by the presence of a supersonic zone which has a tendency to produce the shock wave in the vicinity of 70% of the chord. Contrary to this, the symmetry plane flow over the optimal configuration is subsonic, and the sectional loading is shifted in the leading edge direction.

Moving outboard, we note that at $z = 13.0m$ (Fig. 9), the above trend for the baseline configuration has been realized in a strong shock at approximately 55% of the chord length. As this takes place, the height of the corresponding supersonic bell grows and achieves about $35 - 40\%$ of the local chord length. For the optimal configuration (see Fig. 10), the situation is completely different and the shock wave is absent. Though the supersonic bell is also present, the transition of the supersonic flow to the subsonic one occurs in a smooth way. Additionally, similar to the symmetry plane, we observe the shift of the sectional loading in the leading edge direction.

In order to better assess the advantages of different optimization cases, it is interesting to compare the overall aerodynamic performance of the optimized shapes with that of the original aircraft configuration. The natural way to do this is to present drag polars at the design free-stream Mach numbers $M = 0.85$ and $M = 0.87$, the Mach drag rise curve at the design $C_L = 0.41$ and C_L vs. angle of attack curve at $M = 0.20$.

The analysis of drag polars at the main design point (Fig. 11) allows to draw the following conclusions. In all the considered optimization cases, the optimized configurations demonstrate a significant improvement to the original shape in the whole range of lift coefficients. It is important to note that in the wide vicinity of the design lift coefficient, all the polars are very close to each other.

At a higher free-stream Mach number, corresponding to a secondary design point at $M = 0.87$, the above mentioned superiority (in terms of drag) of the optimized configurations over the baseline one, is retained for a wide range of C_L values (see Fig. 12). At the same time, contrary to $M = 0.85$, the three-point optimization $CaseBWB\_3$ has a clear advantage.

Let us turn our attention to the analysis of Mach drag rise curves at $C_L = 0.41$ (Fig. 13). Already the original (baseline) shape possesses reasonably good drag rise characteristics: the total drag value is kept practically constant up to $M = 0.80$ with the Mach drag divergence point located close to $M = 0.82$. Nevertheless, the optimization enables one to both decrease the constant level of drag at subsonic and low transonic Mach numbers and to essentially shift the Mach drag divergence point to a higher Mach zone. As this takes place, the value of the Mach drag divergence point for the one- and two-point optimizations is about $M = 0.855$ while for the three-point optimization this value is as high as $M = 0.87$.

Summing up the analysis of results for high transonic free-stream Mach numbers, it may be concluded that the superiority of the three-point optimization is clearly evident. The final conclusions concerning the feasibility of the optimal shape, may be drawn only upon the aerodynamic performance analysis at the take-off conditions. The corresponding data may be found in Fig. 14, where C_L vs. angle of attack curves at $M = 0.20$ are shown.

It can be observed that the values of C_L^{max} for the optimizations $CaseBWB\_1$ and $CaseBWB\_2$, where the take-off requirements were not included into the optimization goals, were lower than that of the baseline configuration. In turn, where the take-off conditions are taken into account, the corresponding optimizations ($CaseBWB\_3$ and $CaseBWB\_4$) produced shapes which visibly improved the baseline C_L^{max} characteristics.

Finally, based on the above detailed aerodynamic analysis in a wide range of flight conditions, it may be concluded that the three-point optimization possesses the best overall aerodynamic performance.

Let us analyze the connection between the achieved aerodynamic performance of the aircraft and the corresponding optimal shapes. Specifically, it is interesting to reveal the mechanism of drag minimization in terms of geometrical trends in aircraft shape.

First of all one can see that the optimal shapes, obtained in different optimization conditions, are markedly different. Contrary to this, the corresponding total drag values at the main design point are very close to each other. This leads to a simple but very important conclusion: the considered optimization problem is ill-posed. More exactly, this means that small changes in the resulting total drag value may produce significant changes in the corresponding shapes. Practically, essentially different geometrical shapes may yield the same drag value in the small vicinity of the minimum drag. Summing up, it may be concluded: the drag minimization problem has no unique solution.

Mathematically, the ill-posedness of a problem complicates the issue. Practically, the solution of such a problem may produce shapes infeasible from the engineering viewpoint. For example, the optimization may yield an unproducible shape with too small a leading

edge radius or a shape which may be practically constructed but is aerodynamically unacceptable due to flight instability.

To remove the above obstacle, we should improve the well-posedness of the problem. In our case, one of the natural and very efficient ways to do this, is to diminish the dimensions of the search space and thus to exclude from consideration the shapes infeasible from the engineering viewpoint. This may be accomplished by introducing numerous geometrical and aerodynamic constraints into the problem. The required constraints can be naturally derived from the multidisciplinary considerations such as flight stability, material requirements and so on.

The presented results show that the imposition of constraints allows one to reach the stated practical goal: to obtain minimum drag configurations and, at the same time, to avoid infeasible shapes. In particular, the optimal shape of $CaseBWB\_3$ yields the drag value close to the theoretical minimum and complies with the main design requirements coming from the multidisciplinary considerations.

5 CONCLUSIONS

The multiconstrained optimization of a Blended Wing Body configuration for minimum total drag has been considered. The important features of the optimization technology included a new strategy for efficient handling of nonlinear constraints in the framework of Genetic Algorithms, scanning of the optimization search space by a combination of full Navier-Stokes computations with the ROM method, and a multilevel parallelization of the whole computational framework which efficiently makes use of computational power supplied by massively parallel processors. The analysis of a large body of results demonstrates that the developed optimization technique allows for finding the solutions with the performance close to that of the total optimum. The designed shapes which satisfy a large number of aerodynamic and geometrical constraints, are aerodynamically feasible, yield essential aerodynamic improvement to the initial geometry at the main design point alongside good off-design performance. By means of the three-point optimization, we respectively achieved 20% and 29% reduction in drag in the main and a higher Mach secondary design points, while keeping C_L^{max} at the take-off conditions to the required level.

REFERENCES

[1] Northrop, J.K., "The Development of All-Wing Aircraft", *J. R. Aeronaut. Soc.,* Vol. 51, 1947, pp.481-510.

[2] Portsdam, M. A., Page, M. A., Liebeck, R.H., "Blended Wing Body Analysis and Design", *AIAA Paper,* 1997-2317, 1997.

[3] Liebeck, R.H., Page, M. A., Rawdon B.K., "Blended Wing Body Subsonic Commercial Aircraft", *AIAA Paper,* 1998-0438, 1998.

[4] Liebeck, R.H., "Design of the Blended Wing Body Subsonic Transport", *J. of Aircraft,* Vol. 41, No.1, 2004, pp.10-25.

[5] Morris, A.J., "MOB: A European Distributed Multi-disciplinary Design and Optimization Project", *AIAA Paper,* 2002-5446, 2002.

[6] Qin, N., Vavalle, A., Le Moigne, A., Laban, M., Hackett, K., Weierfelt, P., "Aerodynamic Consideration of Blended Wing Body Aircraft", *Progress in Aerospace Sciences,* Vol. 40, 2004, pp.321-343.

[7] *http://www.cfdreview.com/articles/03/10/20/1357201.shtml*

[8] Epstein, B., and Peigin, S., "Constrained Aerodynamic Optimization of 3D Wings Driven by Navier-Stokes Computations" *AIAA Journal*, **43**, No.9, 2005, pp. 1946–1957.

[9] Epstein, B., Rubin, T. and Seror, S., Accurate multiblock Navier-Stokes solver for complex aerodynamic configurations. *AIAA Journal*, **41**, 2003, pp. 582–594.

[10] Shu, C.-W. and Osher, S., Efficient implementation of essentially non-oscillatory shock-capturing schemes. *J. of Comput. Phys.,* **83**, 1989, pp. 32–78.

[11] Seror, S., Rubin, T., Peigin, S. and Epstein, B., 2005, Implementation and Validation of the Spalart-Allmaras Turbulence Model for a Parallel CFD Code, *Journal of Aircraft,* **42**, No.1, 2005, pp. 179–188.

[12] Michalewicz, Z., *Genetic Algorithms + Data Structures = Evolution Programs*, Springer Verlag, New-York, 1996.

[13] Peigin, S. and Epstein, B., Robust handling of non-linear constraints for GA optimization of aerodynamic shapes. *Int. J. Numer. Meth. Fluids*, **45**, 2004, pp. 1339–1362.

[14] Peigin, S., and Epstein, B., 2004, Embedded parallelization approach for optimization in aerodynamic design. *The Journal of Supercomputing*, **29**, 243–263.

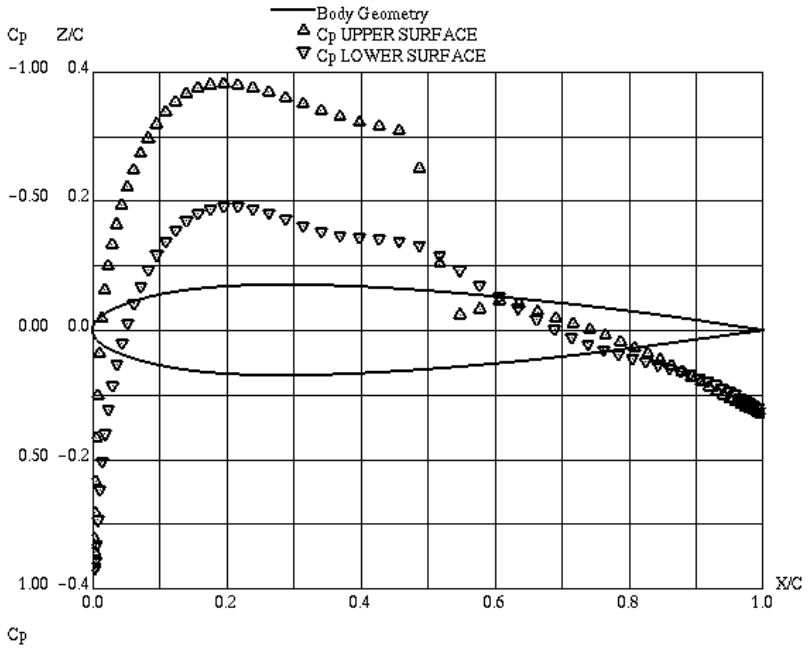

Figure 1: BWB baseline configuration. Streamwise pressure distribution at section $z = 13.0m$. $M = 0.85$, $C_L = 0.41$.

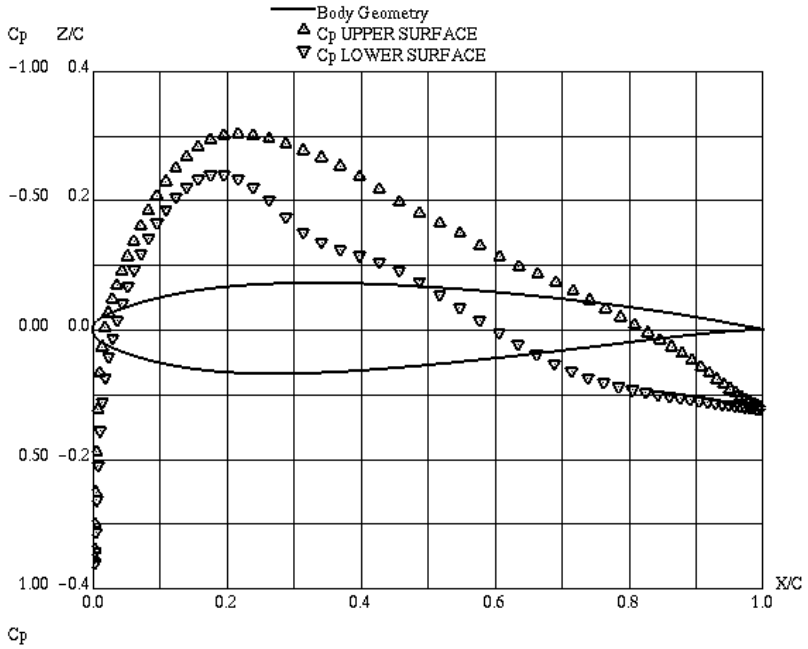

Figure 2: BWB configuration. One-point optimization: $CaseBWB\_1$. Streamwise pressure distribution at section $z = 13.0m$. $M = 0.85$, $C_L = 0.41$.

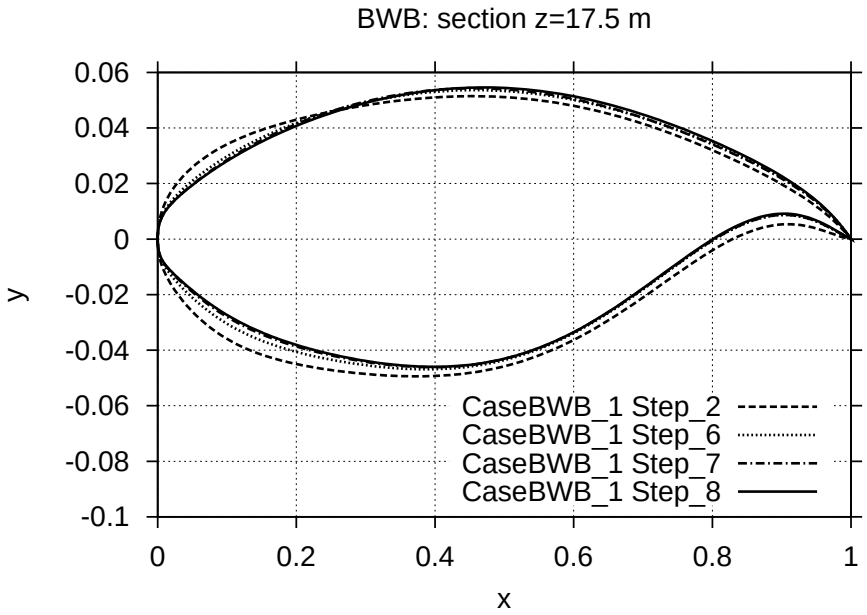

Figure 3: BWB configuration. One-point optimization: $CaseBWB\_1$. Shape of section at $z = 17.5m$ for different optimization steps.

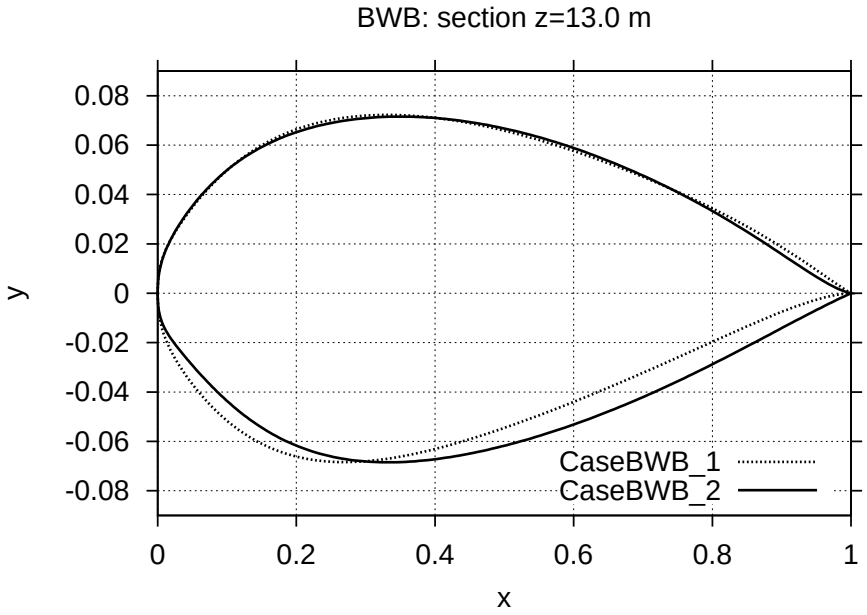

Figure 4: BWB configuration. One-point optimizations. Shape of section at $z = 23.5m$. $CaseBWB\_1$ vs. $CaseBWB\_2$.

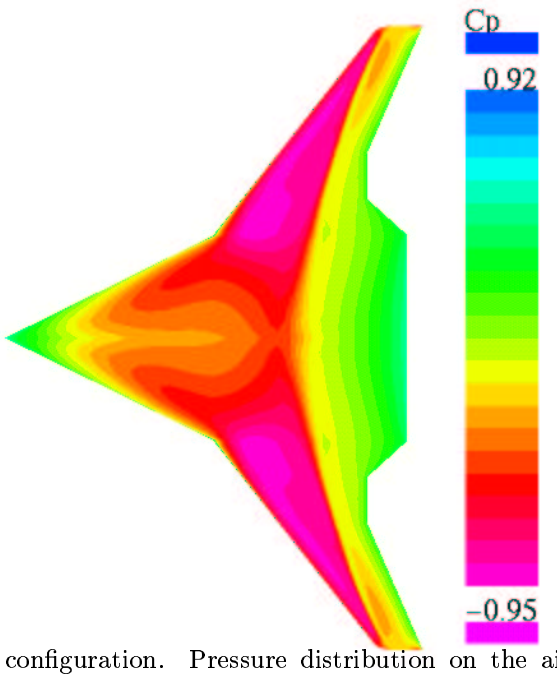

Figure 5: BWB baseline configuration. Pressure distribution on the aircraft surface at $M = 0.85$, $C_L = 0.41$.

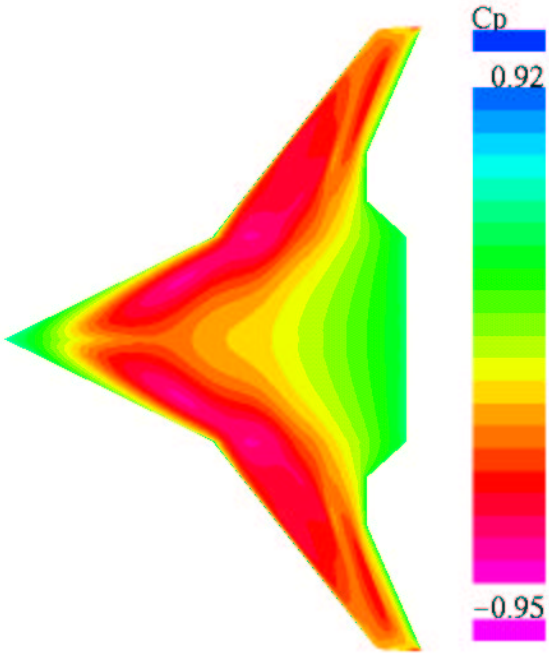

Figure 6: BWB configuration. Multipoint optimization: $CaseBWB\_3$. Pressure distribution on the aircraft surface at $M = 0.85$, $C_L = 0.41$.

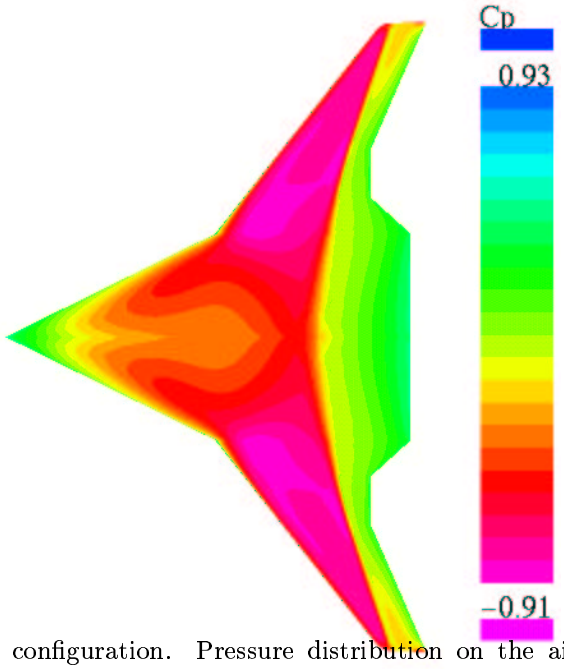

Figure 7: BWB baseline configuration. Pressure distribution on the aircraft surface at $M = 0.87$, $C_L = 0.41$.

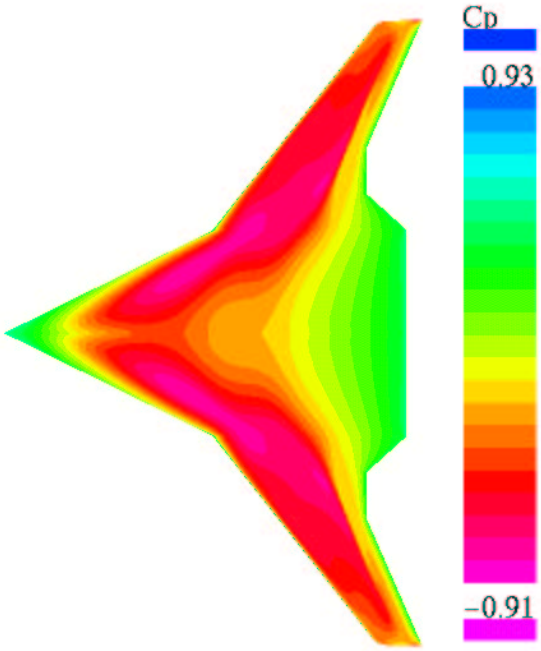

Figure 8: BWB configuration. Multipoint optimization: $CaseBWB\_3$. Pressure distribution on the aircraft surface at $M = 0.87$, $C_L = 0.41$.

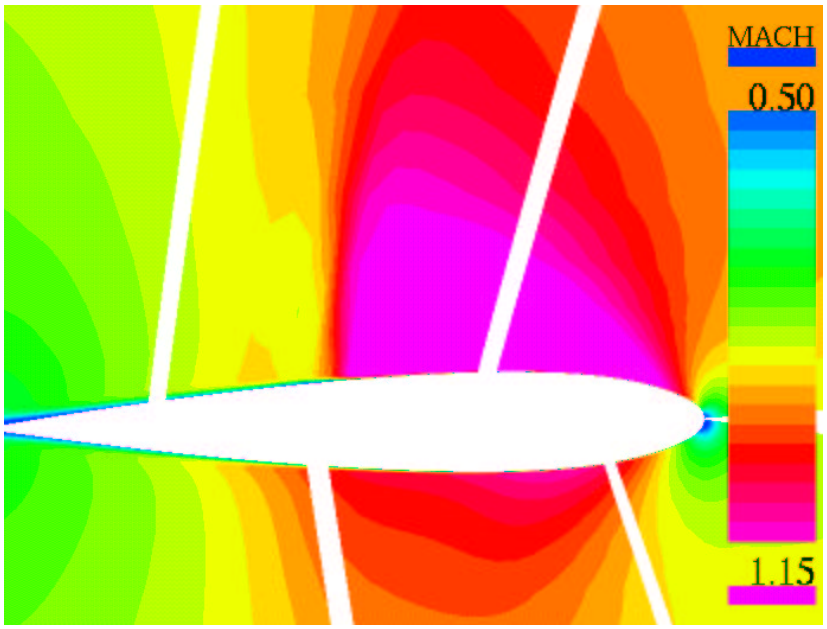

Figure 9: BWB baseline configuration at $M = 0.85$, $C_L = 0.41$. Mach distribution at section $z = 13.0m$

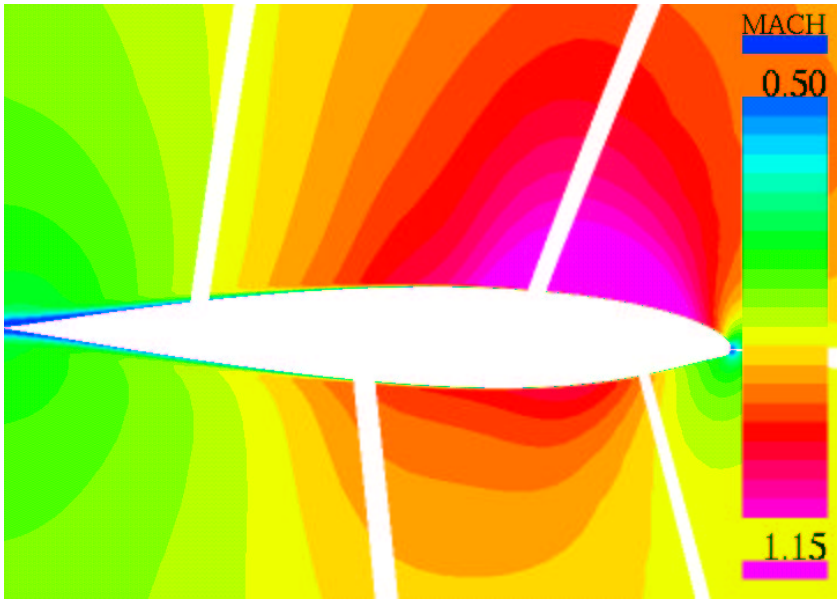

Figure 10: BWB configuration. Multipoint optimization ($CaseBWB\_3$) at $M = 0.85$, $C_L = 0.41$. Mach distribution at section $z = 13.0m$

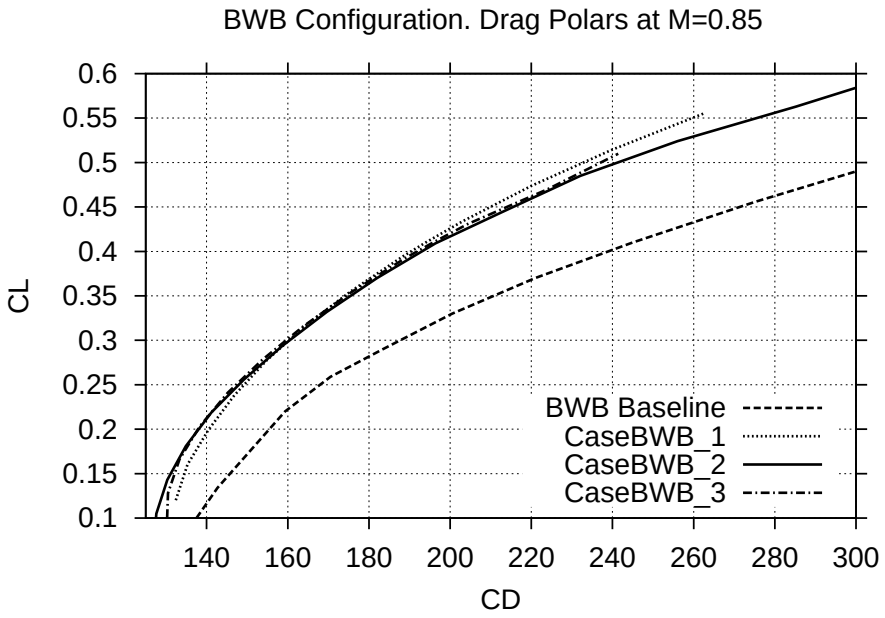

Figure 11: BWB aircraft. Drag polars at $M = 0.85$. Baseline vs. optimal ones.

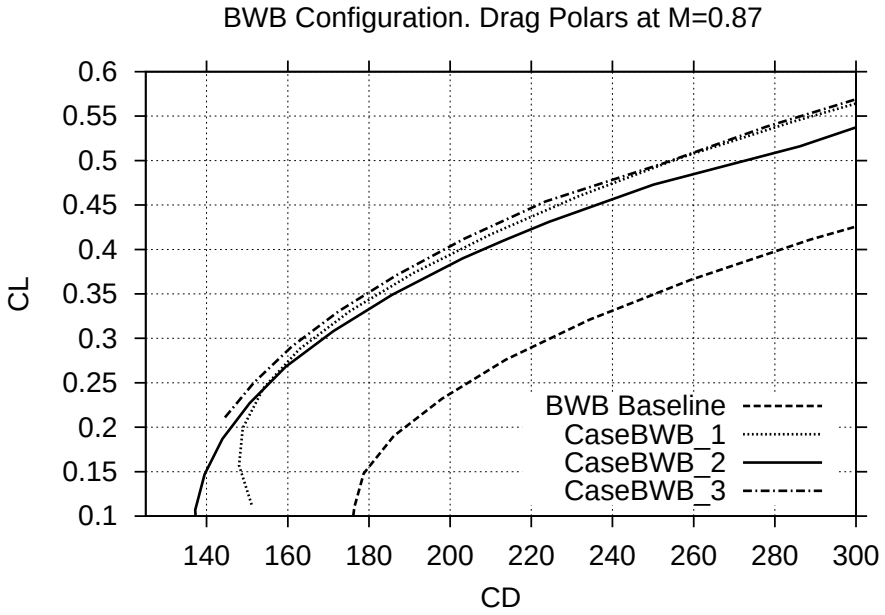

Figure 12: BWB aircraft. Drag polars at $M = 0.87$. Baseline vs. optimal ones.

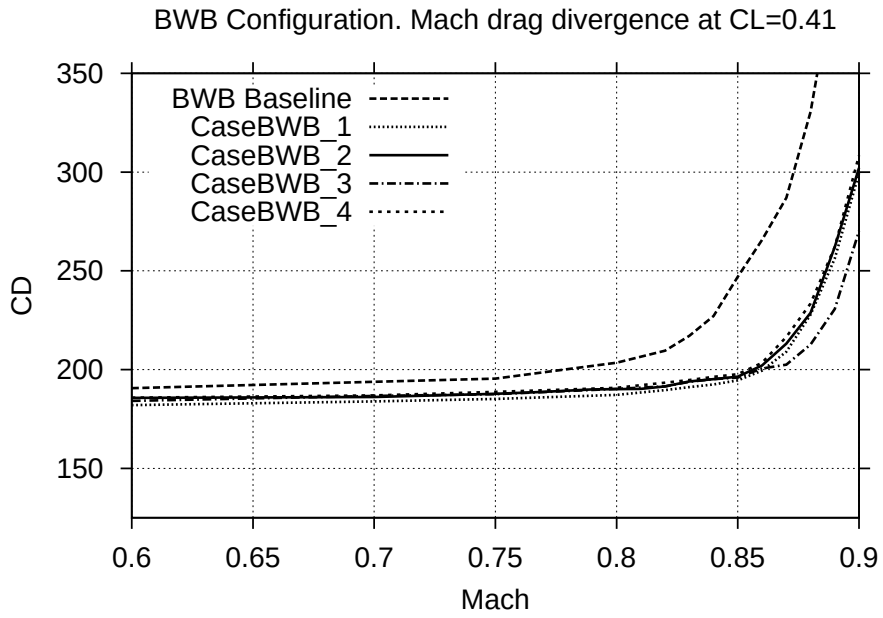

Figure 13: BWB aircraft. Mach drag divergence at cruise lift coefficient $C_L = 0.41$.

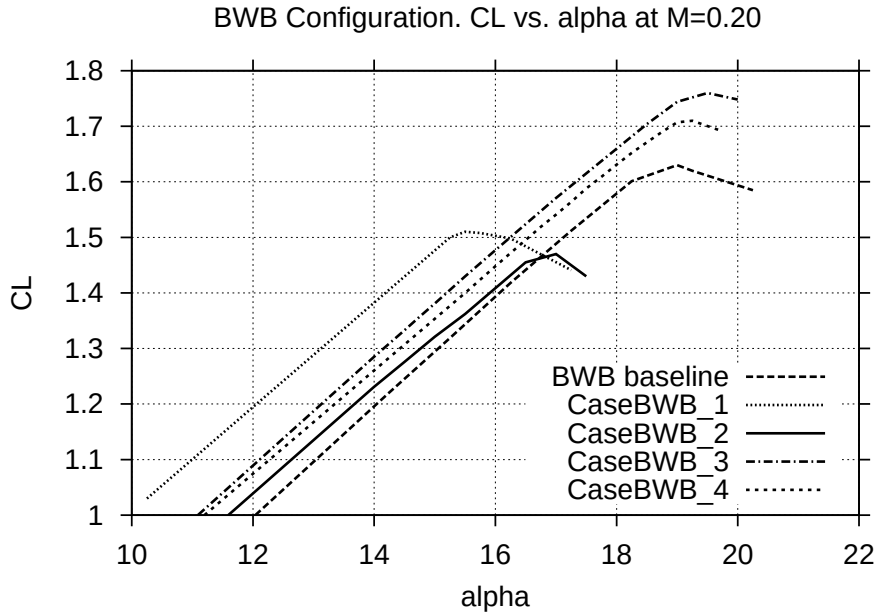

Figure 14: BWB aircraft. Lift coefficient C_L vs angle of attack at take-off conditions ($M = 0.20$).